Supporting Information

Over 20% solar-to-hydrogen efficiency system using a self-reconstructed NiCoFe-based hydroxide nanosheet electrocatalyst and monolithic perovskite/silicon tandem solar cell

*Sanjiang Pan [1,2,3,4†], Renjie Li[1,2,3,4†], Qixing Zhang [1,2,3,4], Chunyu Cui[5], Manjing Wang [1,2,3,4], Biao Shi [1,2,3,4], Pengyang Wang [1,2,3,4], Chaohua Zhang[6], Bo Zhang[5], Ying Zhao [1,2,3,4], Xiaodan Zhang [1,2,3,4]**

Mr. S. Pan, Mr. R. Li, Dr. Q. Zhang, Mr. C. Cui, Miss. M. Wang, Dr. B. Shi, Dr. P Wang, Mr. C. Zhang, Prof. B. Zhang, Prof. Y. Zhao, Prof. X. Zhang

[1] *Institute of Photoelectronic Thin Film Devices and Technology, Renewable Energy Conversion and Storage Center, Solar Energy Conversion Center, Nankai University, Tianjin 300350, PR China*

[2] *Key Laboratory of Photoelectronic Thin Film Devices and Technology of Tianjin, Tianjin 300350, PR China*

[3] *Engineering Research Center of Thin Film Photoelectronic Technology of Ministry of Education, Tianjin 300350, P.R. China*

[4] *Collaborative Innovation Center of Chemical Science and Engineering (Tianjin), Tianjin 300072, China*

[5] *State Key Laboratory of Molecular Engineering of Polymers, Department of Macromolecular Science and Laboratory of Advanced Materials, Fudan University, Shanghai, 200438, China*

[6] *Gold Stone (Fujian) Energy Company Ltd.*

E-mail: xdzhang@nankai.edu.cn

Methods

Chemicals. $NiCl_2{\cdot}6H_2O$ (99.99%, AR, grade) was purchased from Sigma-Aladrich, $FeCl_3{\cdot}6H_2O$ (99.5% AR, grade) from Heowns, $CoCl_2{\cdot}6H_2O$ (99.99% AR, grade), 2,5-Thiophenedicarboxylic acid (98% GC, grade) and N, N-dimethylformamide (DMF) were bought from Aladdin Reagent. All chemicals were used directly without further purification.

Synthesis of NiCoFe-TDC, NiFe-TDC, Ni-TDC. First, DMF (32 ml), ethanol (2 ml) and water (2 ml) were mixed in a 50 ml polytetrafluoroethylene (PE) tube. Then, 129.12mg of 2,5-Thiophenedicarboxylic acid was dissolved into above mixed solution, and then treated with ultrasonic. Subsequently, 0.25 mmol $NiCl_2.6H_2O$, 0.25 mmol $CoCl_2{\cdot}6H_2O$ and 0.25 mmol $FeCl_3.6H_2O$ were added and ultrasonic treatment. The nickel foam (2 cm * 3 cm) was cleaned with hydrochloric acid, deionized water and ethanol successively. After dissolving Ni^{2+}, Co^{2+} and Fe^{3+} salts, the mixed solution was transferred into a 45 ml Teflon vessel and the pretreated nickel foam was quickly put into the solution. The Teflon vessel was kept at 150 ◦C for 12 h under airtight conditions. Finally, the obtained nickel foam was treated with ultrasonic and washed 3 times with deionized water, ethanol, and vacuum drying.

Other catalysts NiFe-TDC and Ni-TDC was prepared according to the similar procedures with different metal ratios at the beginning.

Synthesis of NiCoFe-OH. 0.333 mmol $NiCl_2.6H_2O$, 0.333 mmol $CoCl_2{\cdot}6H_2O$, 0.333 mmol $FeCl_3.6H_2O$ and 1.2 mmol urea were added into 17.5 mL of anhydrous ethanol. After ultrasonic treatment for 50min, the mixture was evenly mixed and put into a 45 ml Teflon vessel and the pretreated nickel foam (2 cm * 3 cm) was quickly put into the solution. The Teflon vessel was kept at 120 ◦C for 12 h under airtight conditions. Finally, the obtained nickel foam was treated with ultrasonic and washed 3 times with deionized water, ethanol, and vacuum drying.

Synthesis of $MoNi_4/MoO_{3-x}$. 0.250 mmol $(NH_4)_6Mo_7O_{24}\cdot 4H_2O$ and 0.270 mmol NH_4F (pH is ~ 6.24) were added into of 10 mL Milli-Q water and 20 mL of anhydrous ethanol. After ultrasonic treatment for 20 min, the mixture was evenly mixed and put into a 45 ml Teflon vessel and the pretreated nickel foam (3 cm * 4 cm) was quickly put into the solution. The Teflon vessel was kept at 150 ◦C for 8 h under airtight conditions. The product was washed with water several times, then dried in an oven at 60◦C to obtain $NiMoO_4$ nanorod arrays on Ni foam as precursor. The $NiMoO_4$ precursor was then subject to the pyrolysis at 350 ◦C for 1.5 h in H_2/Ar (v/v, 10/90) reduction atmosphere to achieve sample $MoNi_4/MoO_{3-x}$.

Preparation of tandem solar cells. Silicon heterojunction (SHJ)-bottom cell was treated with UV-O_3 for 15 minutes. NiO_x is used as the hole transport layer, and its synthesis method is detailed in reference[1]. These synthesized NiO_x nanoparticles were dispersed in deionized water at a concentration of 20 mg ml^{-1} (2000 rpm, 30 s). The $Cs_{0.22}FA_{0.78}Pb(Br_{0.2}I_{0.8})_3$ (50μL) with the concentration of 1.4M was spread on the substrate and spun at 5000 rpm with a ramp rate of 1000 rpm/s for 50 seconds. The methyl acetate (200μL) was dripped onto the substrate with 20 seconds remaining in the spin cycle. The perovskite layer was then annealed at 100℃ for 30 minutes. A 20nm C_{60} was formed by evaporation and a 20nm SnO_2 was deposited by atomic layer deposition (ALD). Subsequently, an 100nm IZO was deposited by sputtering. A 100 nm silver frame collects charge carriers through thermal evaporation of a shadow mask. Finally, polydimethylsiloxane as an antireflective coating.

Characterization. Powder X-ray diffraction (PXRD) data were conducted on a PAN alytical X'Pert Pro Diffractometer operating at a voltage of 40 kV and a current of 40 mA with Cu Ka radiation (λ= 1.5418 A) from 10 to 80 degrees (2θ). Field emission scanning electron microscopy (FESEM) observations were gathered on a Hitachi S-4800 microscope performing at an accelerating voltage of 20.0 kV. Transmission electron microscopy (TEM) images were collected with a JEOLJEM-2010 instrument operating at 200 kV. X-ray photoelectron spectroscopy (XPS) spectra were acquired with ESCALab220i-XL electron spectrometer. FEI SEM operated at 1.5 kV was used to characterize the surfaces of the samples. The EXAFS data were

collected on the 1W1B beamline at the Beijing Synchrotron Radiation facility. Fourier transform infrared spectroscopy spectra (FTIR) were collected on a FT-IR spectrometer (Bruker Tensor 27) with a range of 400-4000 cm^{-1} at room temperature. The atomic composition of samples was determined using an Inductively Coupled Plasma Optical Emission Spectrometry (ICP-OES). The current-voltage characteristics of the devices were measured by a Keithley 2400 Source meter under AM 1.5G illumination with a xenon-lamp-based solar simulator (Enli. Tec., Taiwan). The external quantum efficiency (EQE) spectra was recorded in direct current (DC) modeusing EQE system (QEX10, PV Measurement Co, Ltd.).

Electrochemical measurement of OER activities. Electrochemical measurements were performed using a three-electrode system connected to an electrochemical workstation (Autolab PGSTAT302N) with a built-in EIS analyzer. The working electrode was fabricated using the in-situ growth method on Ni foam (area: 0.5 cm^{-2}). Ag/AgCl (with saturated KCl as the filling solution) and platinum sheet were used as the reference and counter electrodes, respectively. The current density (*j*) versus potential (*U*) curves were obtained with a sweep rate of 1 mV s^{-1} from 1.0 V-1.6 V (vs. RHE), in 1 M KOH. EIS measurements were conducted in a static solution at 1.43 V (vs. RHE). The amplitude of the sinusoidal wave was 10 mV, and the frequency scan range was from 100 kHz to 1 Hz. The C_{dl} of electrocatalysts was used to evaluate the ECSA, which was measured by using cyclic voltammograms in a no Faradaic reaction potential window (0.19-0.29 V) with the scan rates of 20, 40, 60, 80, 100 and 120 mV s^{-1}, respectively. The plot of the current density differences ($\triangle J = (J_1 - J_2)/2$ at 1.04 V vs. RHE) against the different scan rates yields a straight line, whose slope is C_{dl}. The ECSA was calculated by ECSA= C_{dl}/C_s, where C_s is the specific capacitance using an average value of 0.04 mF cm^{-2}. The experimental condition of photovoltaic-driven water splitting system without any encapsulation was kept at 25 °C and an ambient air (~20% RH) during the overall measurement. Unless otherwise stated, all experiments were performed at ambient temperature (25 ± 2 °C), and the electrode potential was converted to the RHE scale using the equation：

$$E(RHE) = E(Ag / AgCl) + 0.197V + 0.059 \times PH \quad (1)$$

IR correction. The correction was done according to the given equation:

$$E_{corrected} = E - iR \quad (2)$$

where $E_{Corrected}$ is the *i*R-corrected potential, E is the experimentally measured potential and R is the series resistance of measurement.

TOF calculations. The TOFs of these catalysts were calculated using the following equation[2]:

$$TOF = \frac{J \times A \times \eta}{4 \times F \times n} \quad (3)$$

J is obtained at iR-corrected overpotential = 300 mV, normalized by geometric area of carbon cloth (0.5 cm^2); R is the series resistance obtained from the fitting of EIS. A is the geometric area of carbon cloth (0.5 cm^2). F is the Faraday constant and η is the Faradaic efficiency. n is the mole number of nickel, cobalt and iron atoms on the electrode., calculated based the integration of catalyst redox features from CV curves.

STH Efficiency Calculation. For the overall water splitting system that produces hydrogen and oxygen molecules using only solar power as the input, the solar-to-hydrogen efficiency (STH) is defined as:

$$STH = \frac{j_{op} \times A \times E_f \times FE_{H_2}}{P_S \times A} \times 100\% \quad (4)$$

Here, j_{op} represents the operating current density of the combined system, A is the effective illuminated area, E_f is the standard thermodynamic potential difference between hydrogen evolution and oxygen evolution half-reactions (1.23 V) that is corresponded to the change of Gibbs free energy of overall water splitting, FE_{H_2} is the faradic efficiency for hydrogen evolution that is assumed to be 100% and P_s is the power of solar illumination.

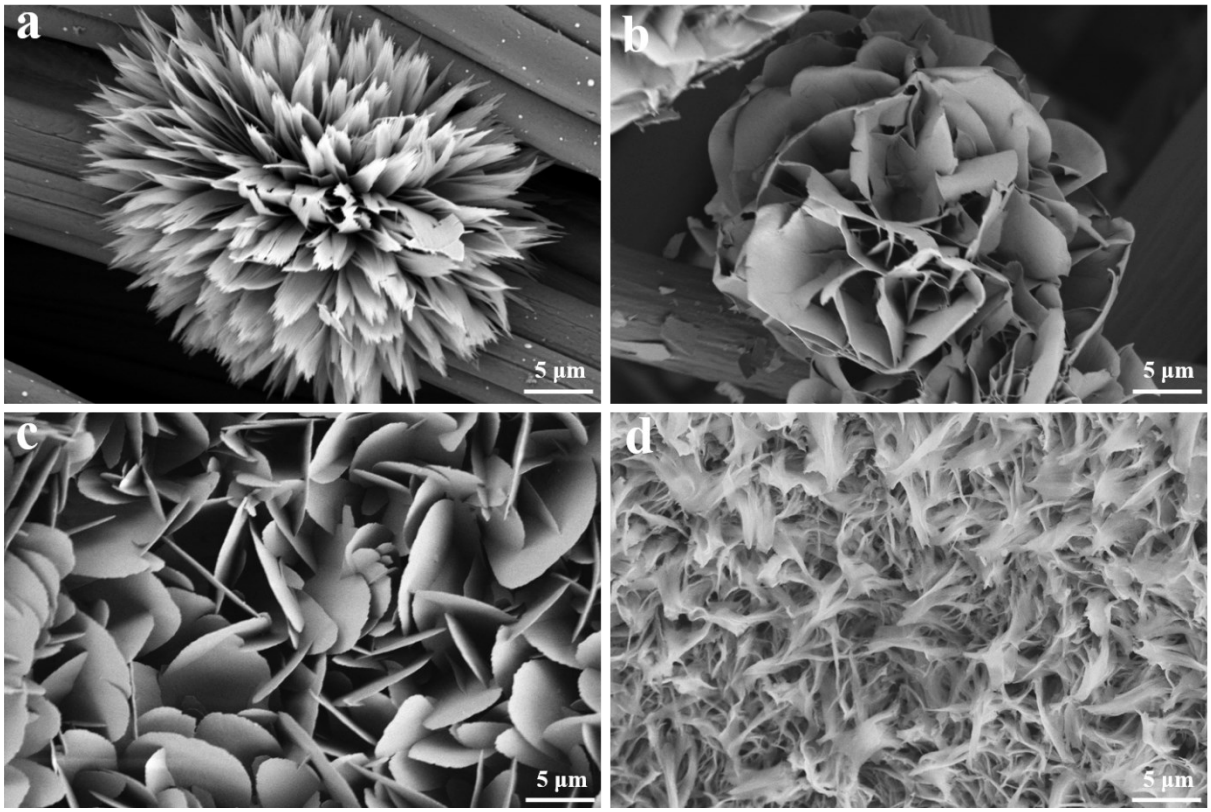

Fig. S1 SEM image of Ni-TDC (a), Ni-TDC-AC (b), NiFe-TDC (c) and NiFe-TDC-AC (d).

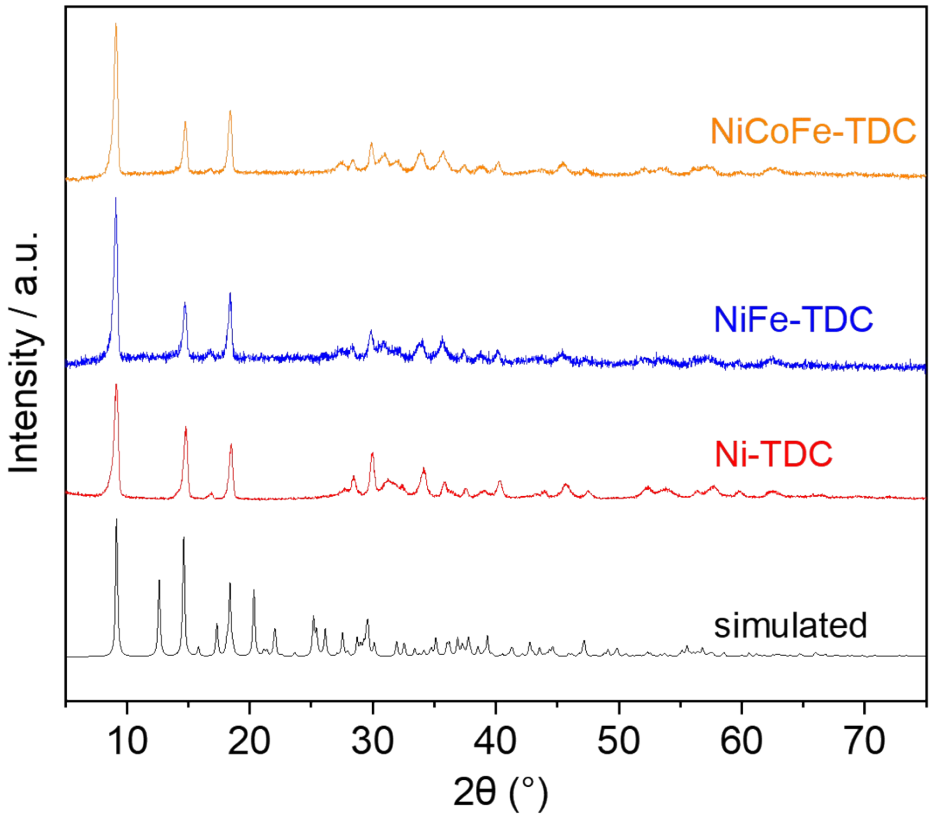

Fig. S2 XRD spectra of NiCoFe-TDC, NiFe-TDC and Ni-TDC. Comparing with the simulated XRD pure spectra of Ni-TDC.

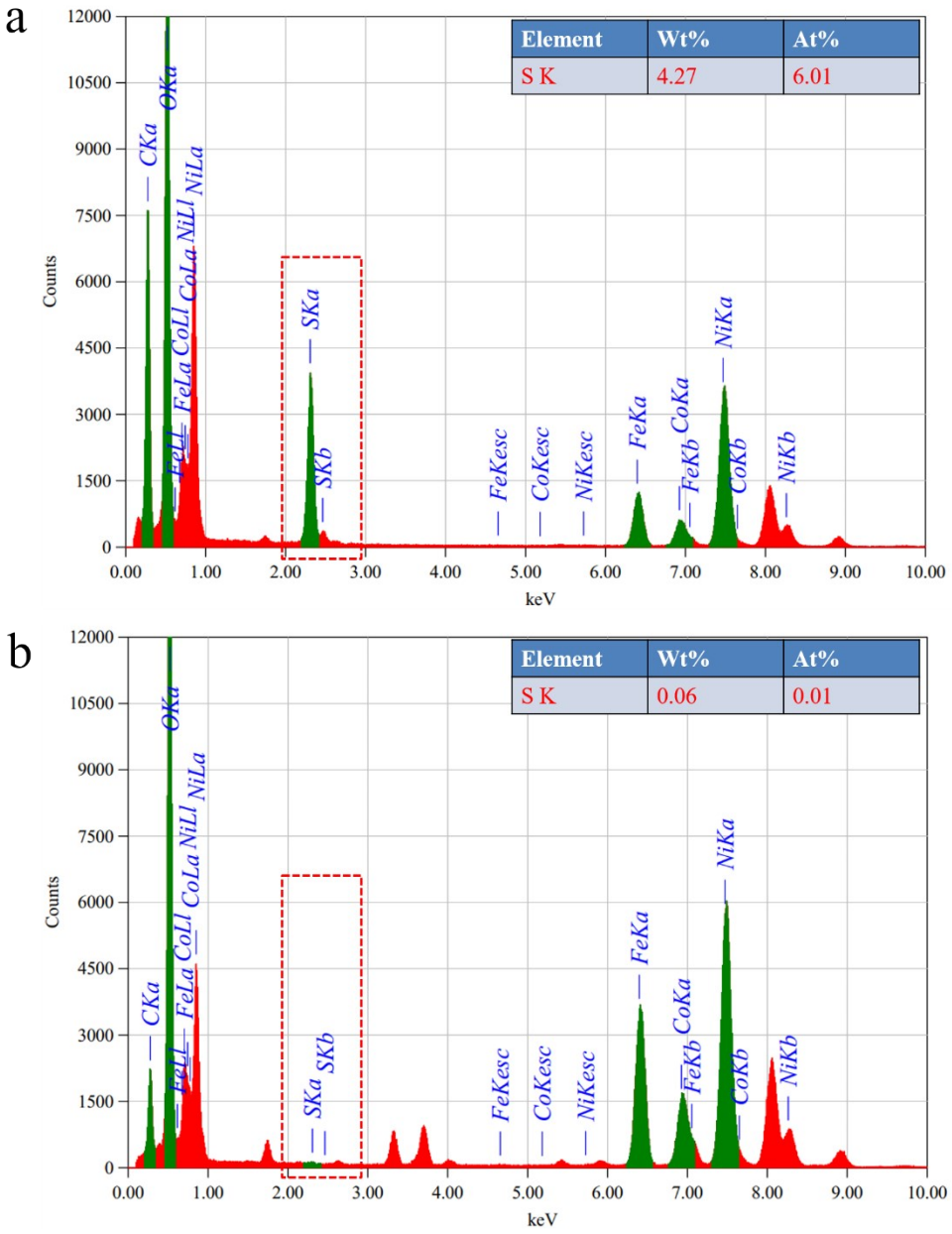

Fig. S3 EDS spectra of NiCoFe-TDC (a) and NiCoFe-TDC-AC (b).

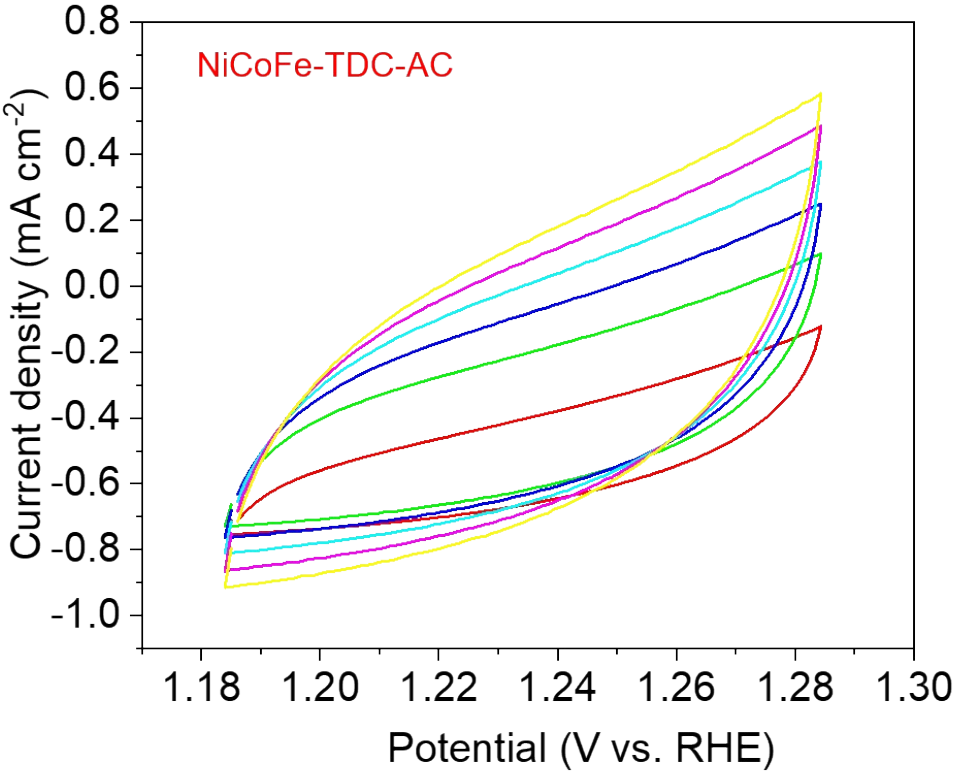

Fig. S4 Typical CV curves of NiCoFe-TDC-AC.

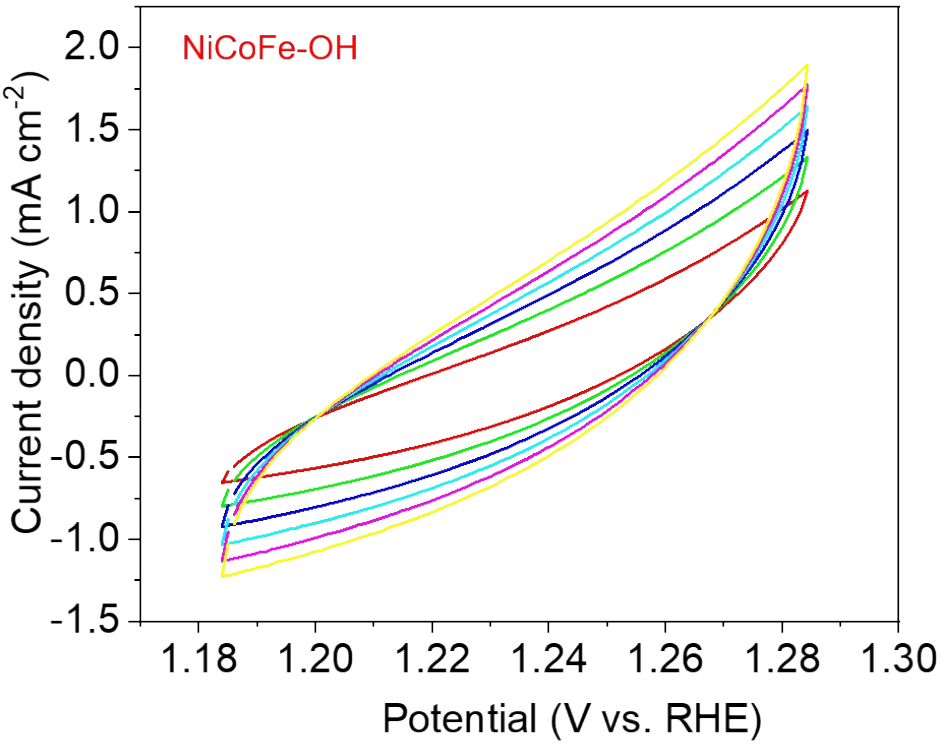

Fig. S5 Typical CV curves of NiCoFe-OH.

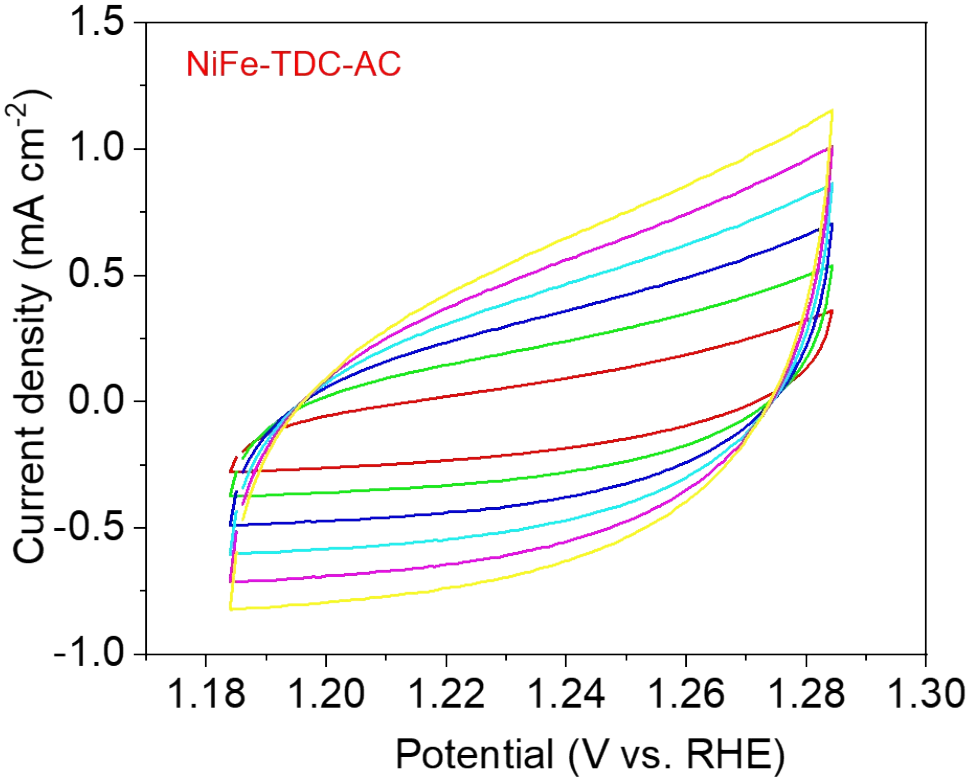

Fig. S6 Typical CV curves of NiFe-TDC-AC.

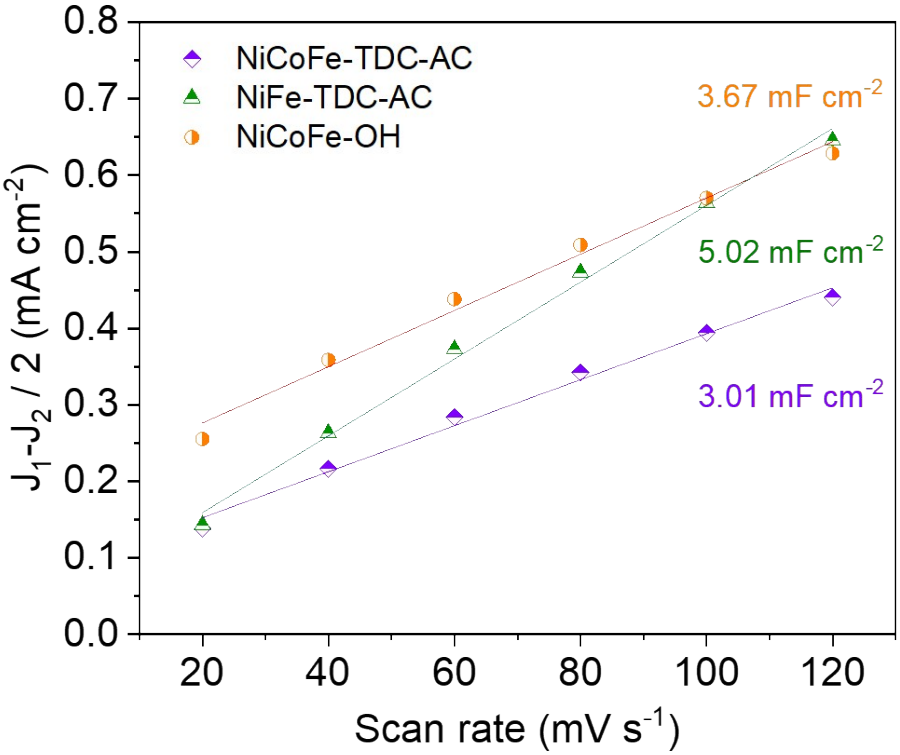

Fig. S7 The fitting plots showing C_{dl} for NiCoFe-TDC-AC, NiFe-TDC-AC and NiCoFe-OH.

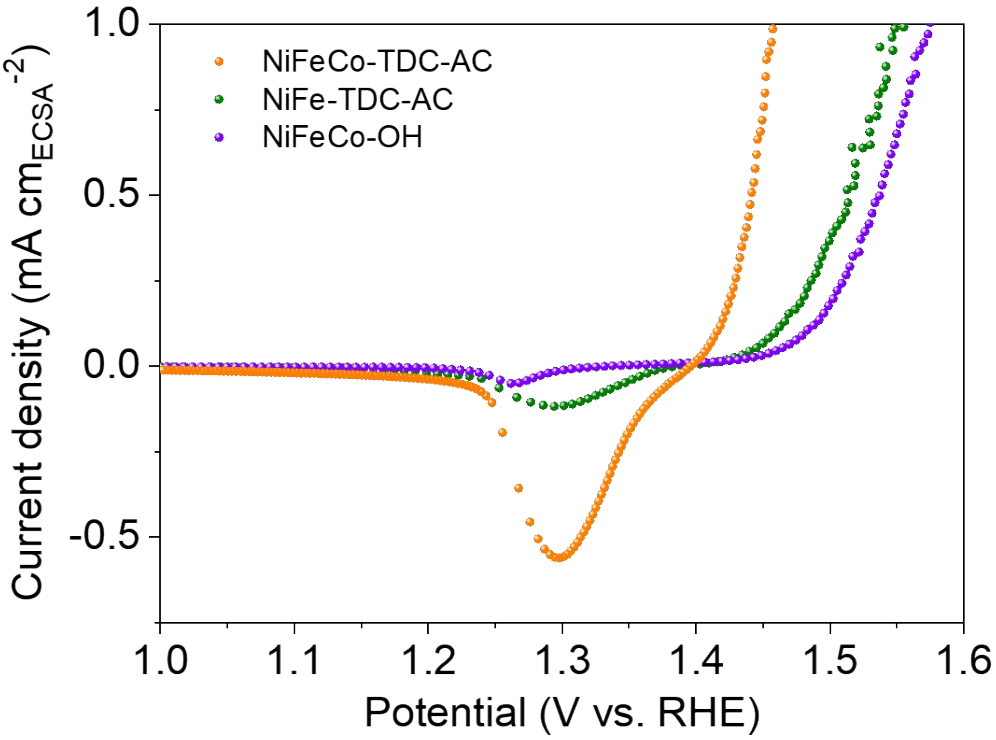

Fig. S8. Polarization curves normalized by the ECSA.

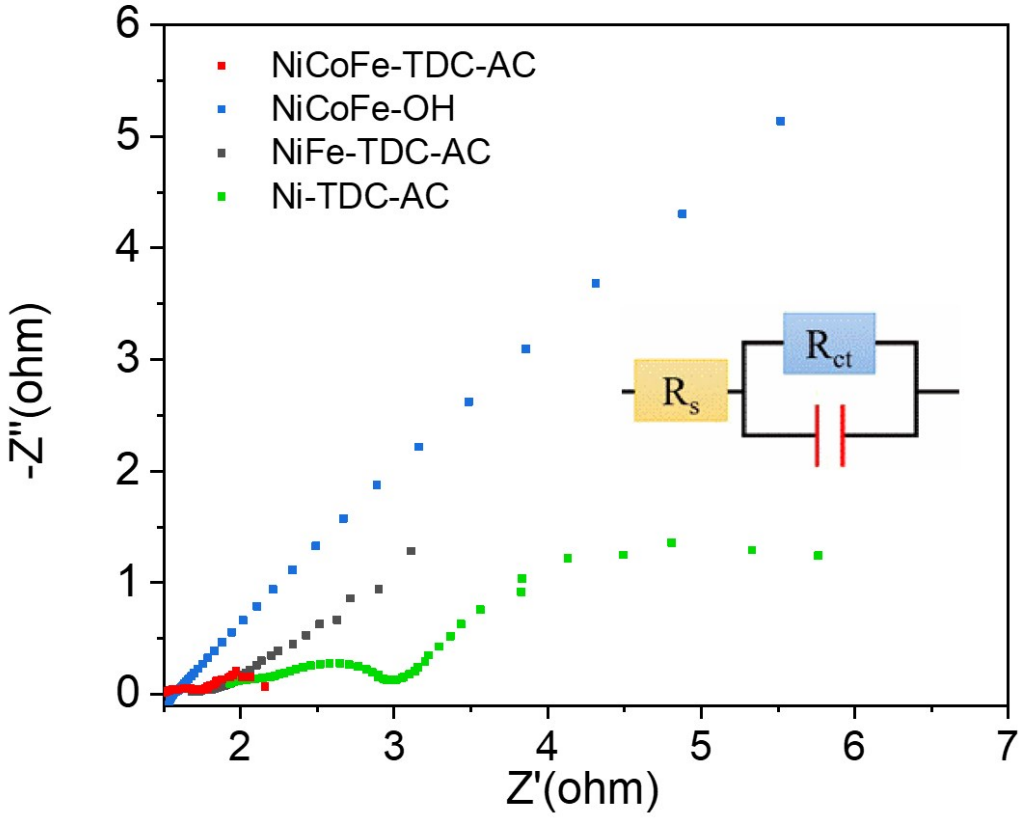

Fig. S9 EIS Nyquist plots of NiCoFe-TDC-AC, NiFe-TDC-AC, Ni-TDC-AC and NiCoFe-OH.

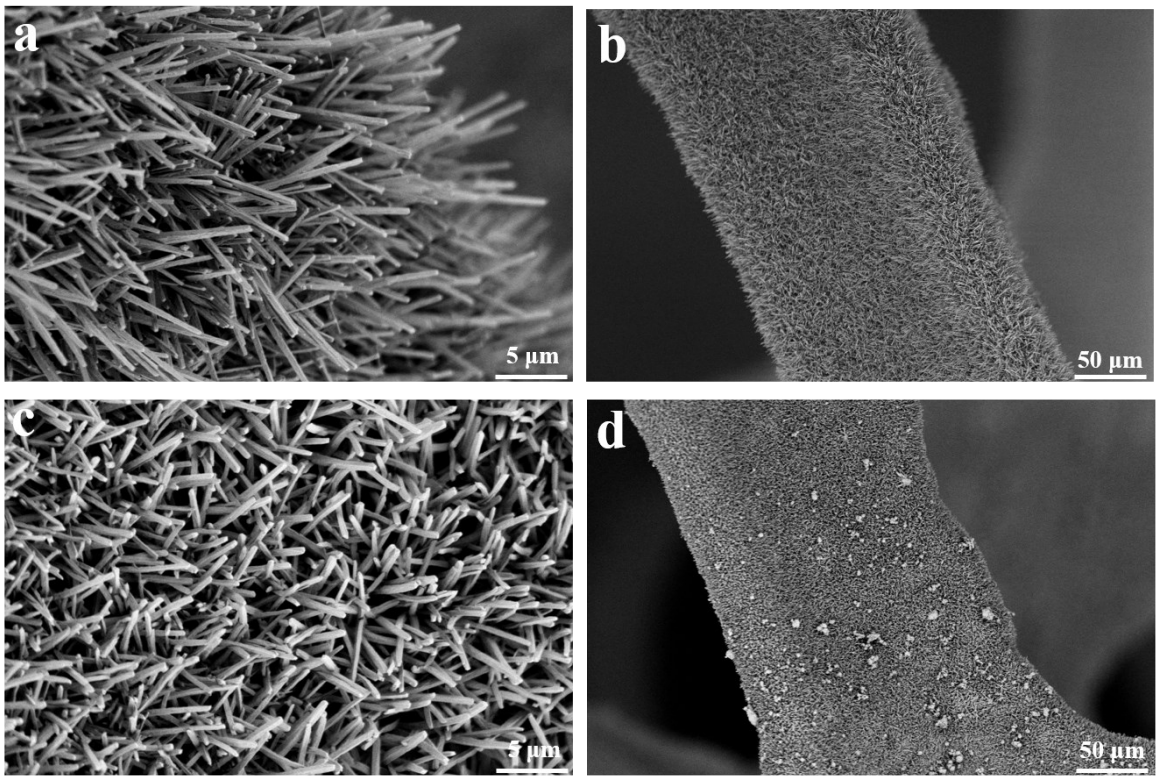

Fig. S10 SEM image of $NiMoO_4$ (a) and (b), $NiMo_4/MoO_{3-X}$ (c) and (d).

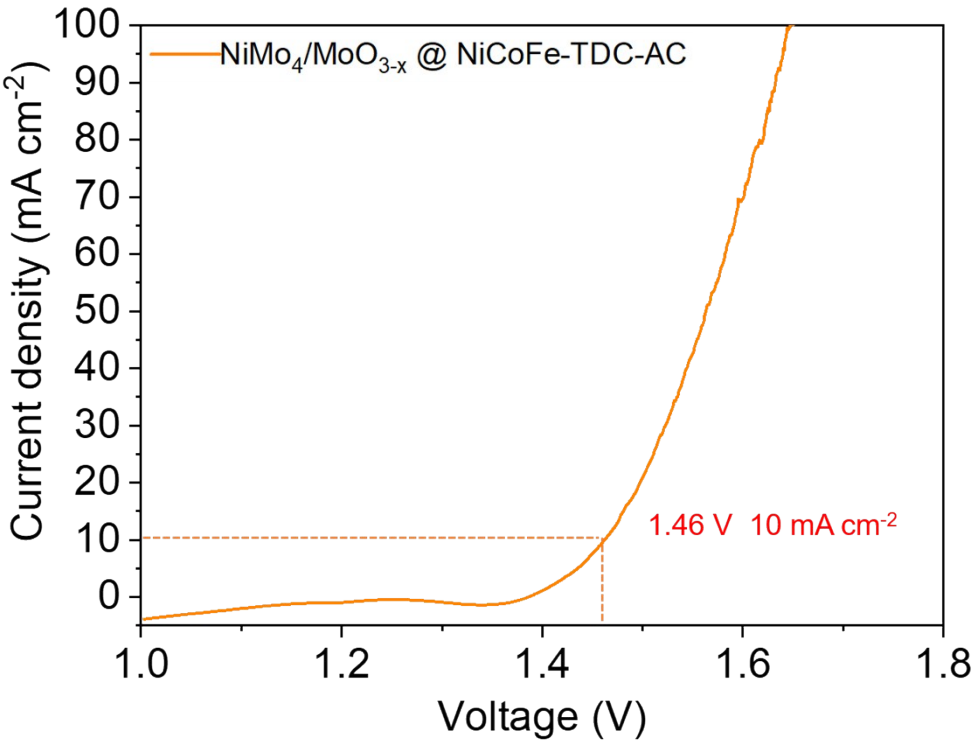

Fig. S11 LSV curve of NiCoFe-TDC-AC and $NiMo_4/MnO_{3-X}$ electrodes based two-electrode configuration in 1 M KOH without iR correction.

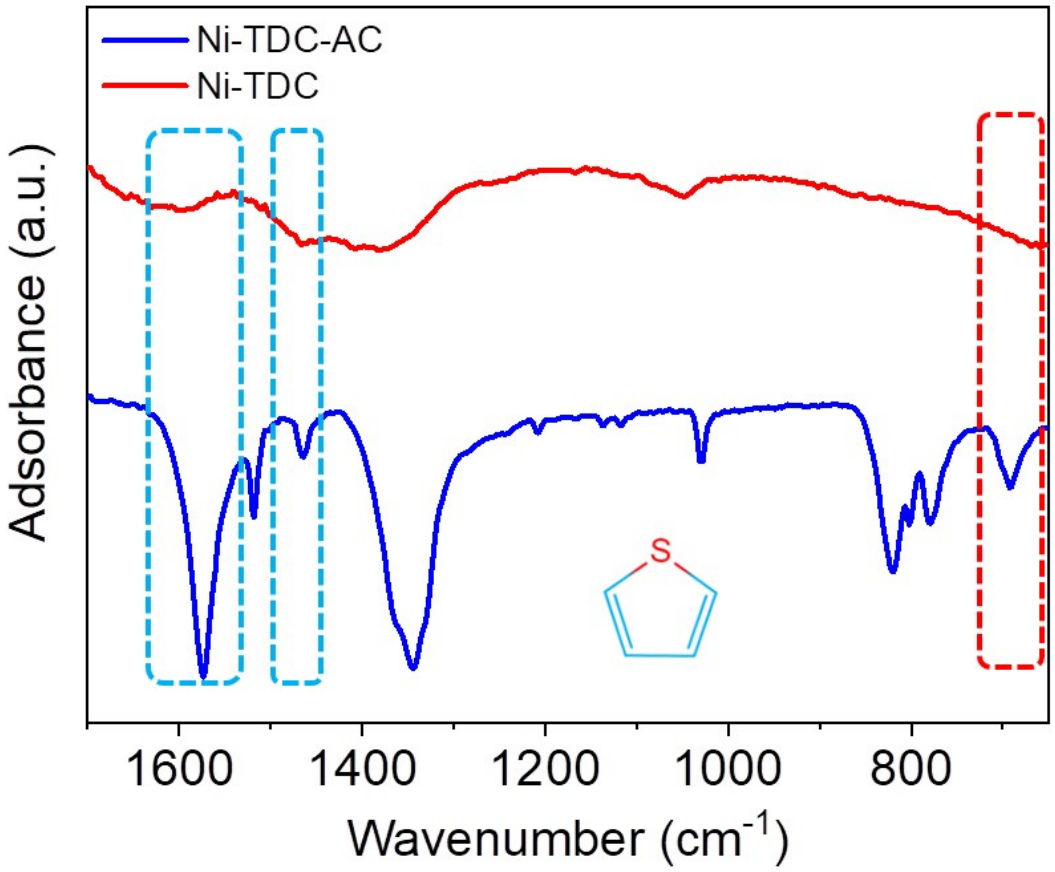

Fig. S12 Fourier transform infrared spectra of Ni-TDC and Ni-TDC-AC.

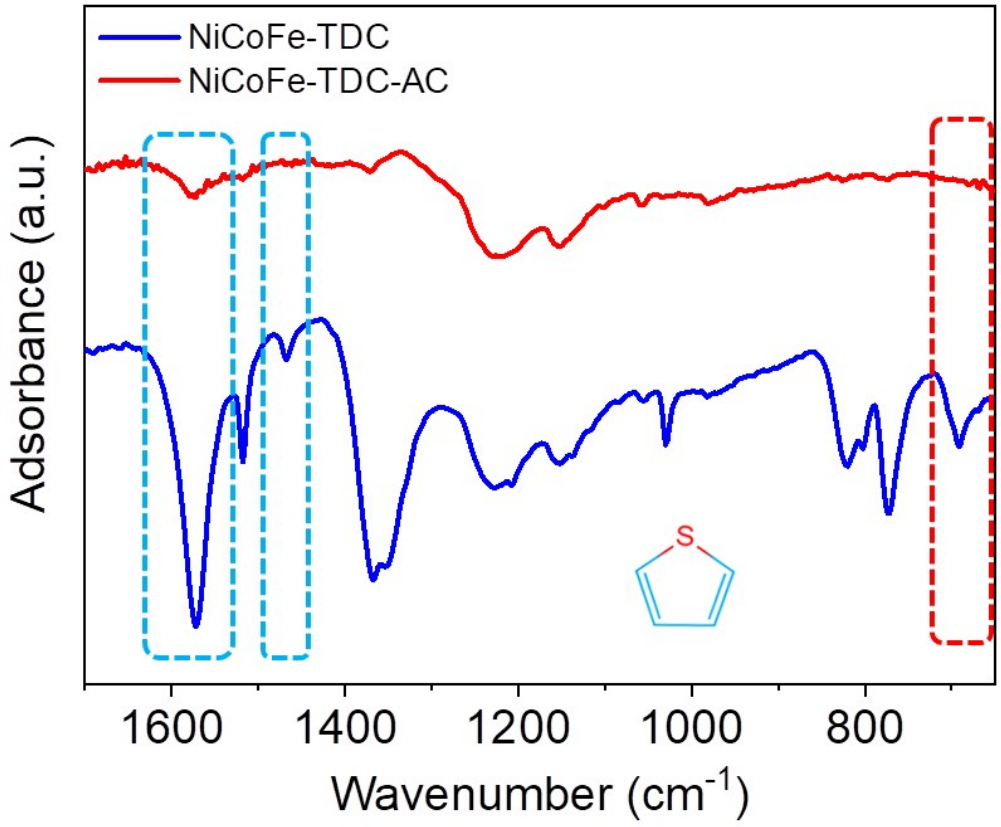

Fig. S13 Fourier transform infrared spectra of NiCoFe-TDC and NiCoFe-TDC-AC.

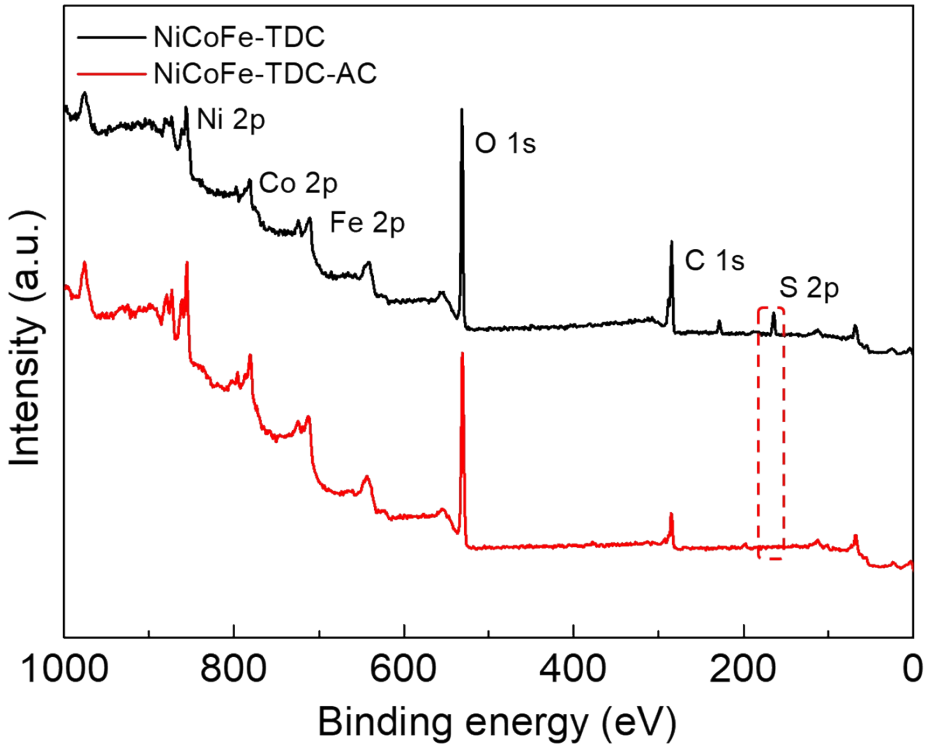

Fig. S14 Full range XPS spectra of NiCoFe-TDC and NiCoFe-TDC-AC.

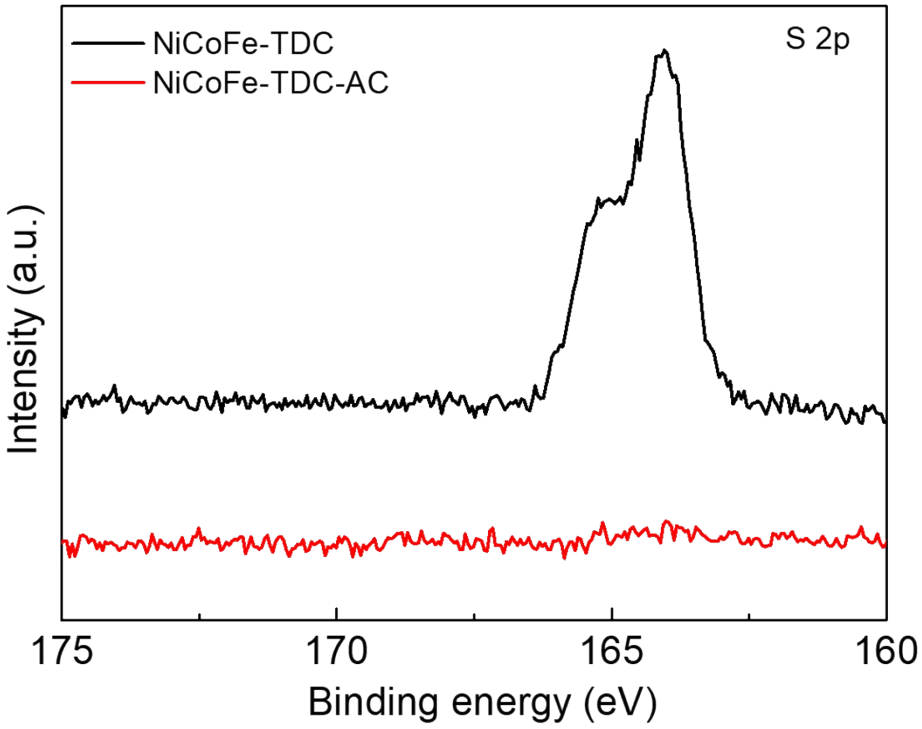

Fig. S15 XPS High resolution S 2p spectra of NiCoFe-TDC and NiCoFe-TDC-AC.

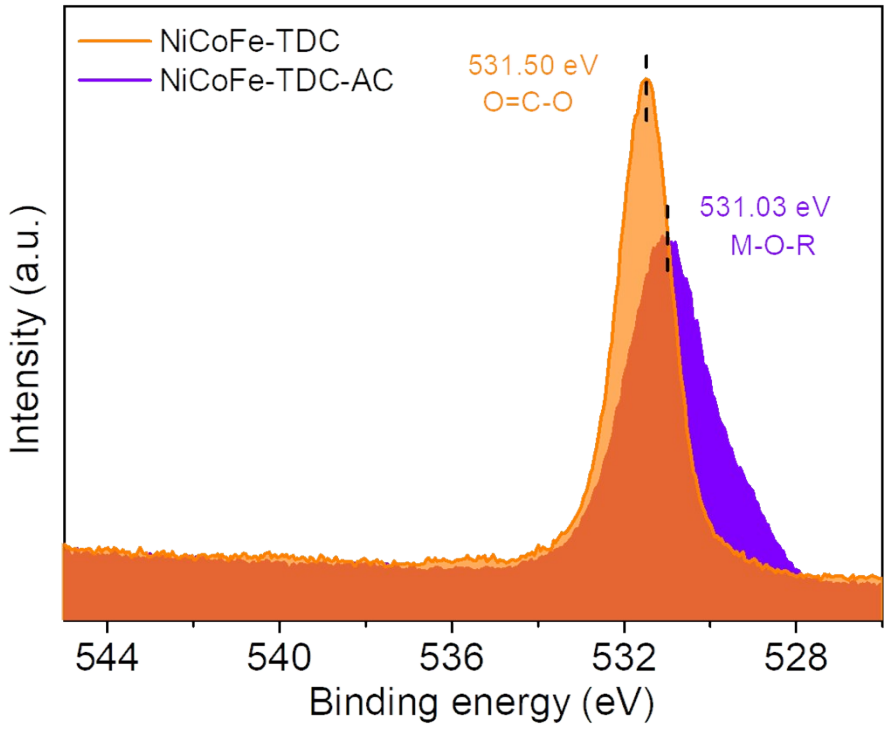

Fig. S16 XPS High resolution O 1s spectra of NiCoFe-TDC and NiCoFe-TDC-AC.

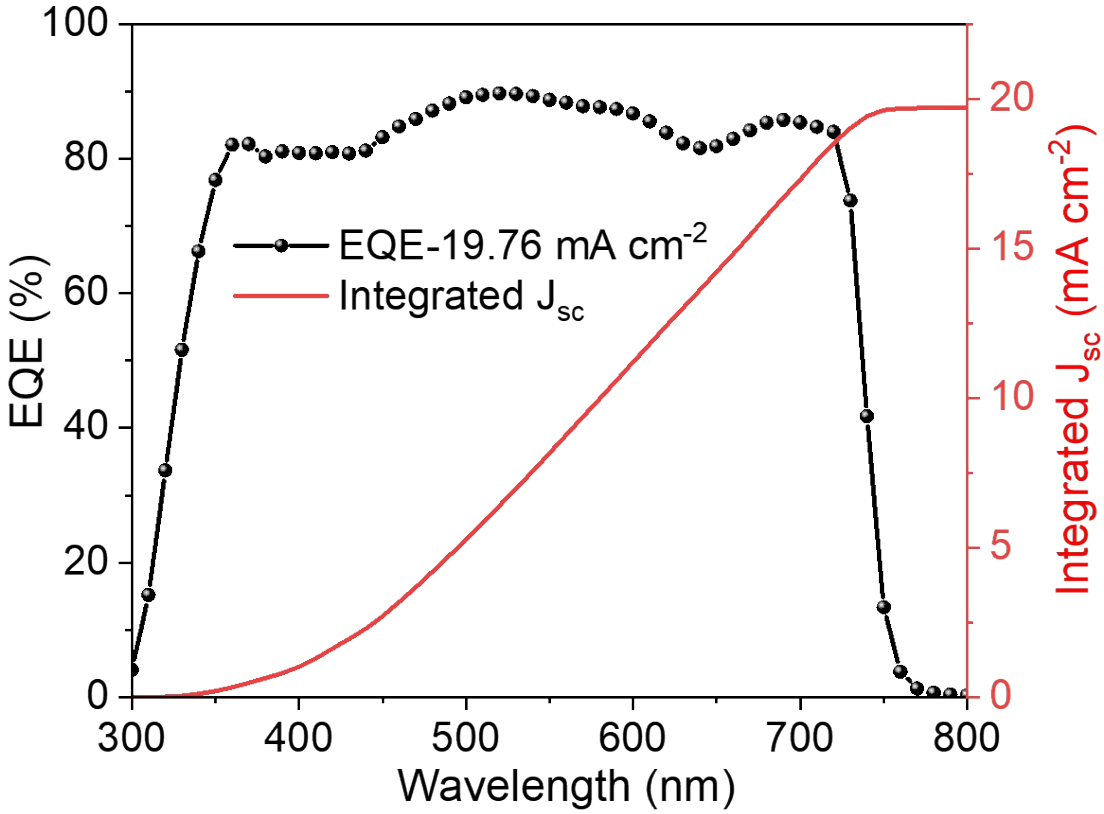

Fig. S17 External quantum efficiency (EQE) of the perovskite cell. The AM1.5G-equivalent current densities are given.

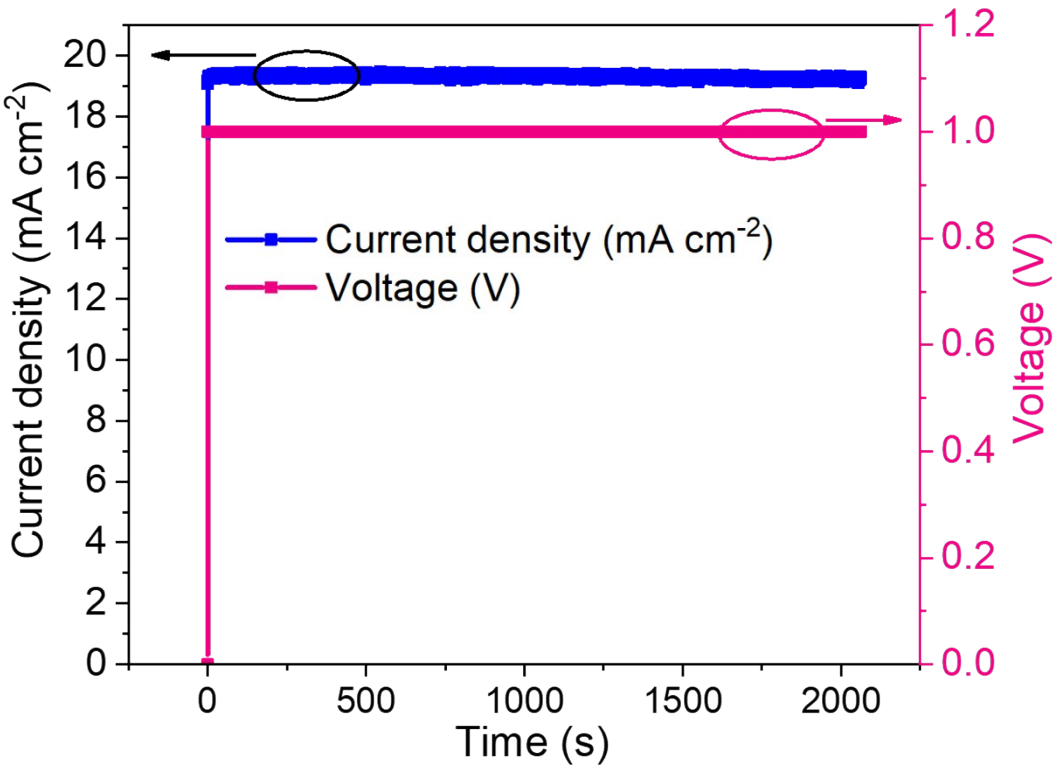

Fig. S18 Maximum power point (MPP) tracking of the perovskite cell for 2000 S.

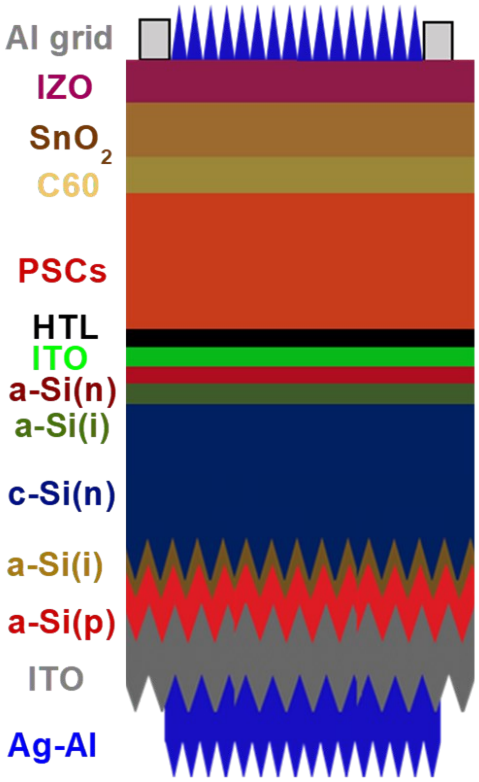

Fig. S19 Schematic view of a monolithic perovskite/Si tandem solar cell.

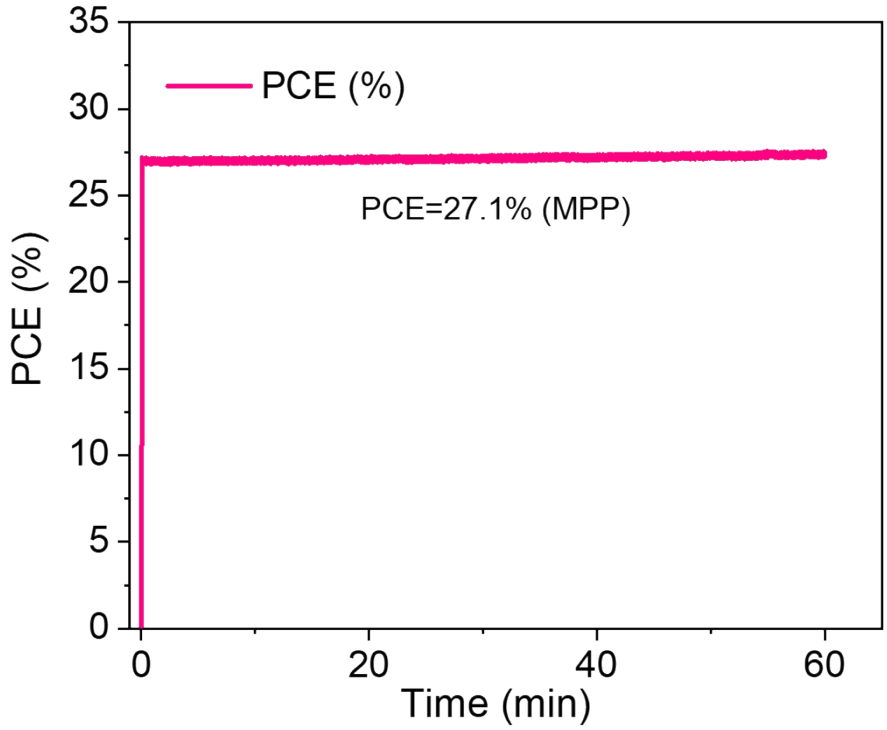

Fig. S20 Maximum power point (MPP) tracking of the perovskite cell for 60min after the 8h water splitting experiment.

Table S1 A summary of STH conversion efficiency and durability of recent low-cost photovoltaic (PV) driven water splitting systems.

PV type	Illumination area/intensity	Electrolyzer, catslysts cathode /anode	Imersed in electrolyte or wired*	Electrolyte	STH efficiency	Durability	Refere nce
Si minimodule (4 single-junction modules series connected)	6 cm^2 1 sun	EC cell, NiMoZn/NiB	Wired	0.5 M KBi/0.5 M H_2SO_4 (pH 9.2)	10.0%	168 h	3
3 Interconnected Si HJ	5.7 cm^2 1 sun	MEA electrolyzer, Pt/IrO_2	Wired	water (pH 7)	14.2%	100 h	4
3 Interconnected Si HJ	5.7 cm^2 1 sun	EC cell, Ni/Ni	Wired	1 M KOH (pH 14)	14.5%	100 h	4
PBDTTPD:PCBM/PED OT:PSSS, 3-junction	0.1 cm^2 1 sun	EC cell, Pt/Ni	Wired	1 M NaOH	6.1%	Not reported	5
PCDTBT/PMDPP3T/PMDPP3T, 3-junction	0.1 cm^2 1 sun	NiMoZn/Co_3O_4 or RuO_2-RuO_2	Integrated and imersed in electrolyte	1 M NaOH	5.4% for RuO_2-RuO_2 4.9% for NiMoZn/Co_3O_4	20 min	6
Tandem DSSC, 4-termianl	0.141 cm^2 0.5 sun	EC cell, Pt/Pt	Wired	0.1 M NaOH	5.75%	5 h	7
2 Serie-connetect PSC	0.32 cm^2 1 sun	BPM electrolyzer, CoP/NiFe LDH	Wired	0.5 M H_2SO_4 in cathode (pH 0.9) and 1 M KOH in anode (pH 13.6)	12.7%	16 h	8
2 Serie-connetect PSC	0.318 cm^2 1 sun	EC cell, NiFe LDH/NiFe LDH	Wired	1 M NaOH (pH 14)	12.3%	10 h	9
Monolithic perovskite/Si tandem solar cell	1.42 cm^2 1 sun	EC cell, CC-TiC Pt/NiFe LDH	Wired	1 M KOH	18.2%	150 min	10
Monolithic perovskite solar cell – connetect p+nn+ -Si/Ti/Pt photocathode	11.5 cm^2 1 sun	EC cell, Pt/ Ir and Ru coated Ti plate	Wired	1 M H_2SO_4	17.6%	400s	11
3 Interconnected Si HJ	4 cm^2 1 sun	EC cell,Cu,NiFe-LDH /NiFe-LDH	Wired	1 M KOH	11.3%	30 h	12
Monolithic perovskite/Si tandem solar cell	0.1875 cm^2 1 sun	EC cell,NiFe-LDH /NiFe-LDH	Wired	1 M KOH	17.52%	450 s	13
Two perovskite tandem cells	0.24 cm^2 1 sun	EC cell, NiFe@NiS_x/NiFe@ NiS_x	Wired	1 M KOH	11.9%	20 h	14
Monolithic perovskite/Si tandem solar cell	**0.5 cm^2 1 sun**	**EC cell, $NiMo_4/MoO_{3-x}$ /NiCoFe-TDC-AC**	**Wired**	**1 M KOH**	**21.32%**	**520 min**	**This Work**

*Note: This table is categorized according to the absorber type and illumination intensity. For photovoltaic (PV) driven water splitting systems, there are mainly two types. One is “wired system” that the photovoltaic cell is connected with electrocatalysts that are immersed in the electrolyte using metal wires, while the PV cell is outside of the electrolyte. The second type is “integrated or wireless system” that the PV cell is either coated with protection layer o encapsulated and connected with electrocatalysts in a “wireless” way (sometimes wires are hidden as close contact) and immersed in the electrolyte. Except the external looking, these two types have no difference in nature as they all rely on the solid-state junction in the PV for the charge separation distinct to the photoelectrochemical (PEC) approach that the charge separation is driven by the semiconductor and electrolyte junction.

Table S2 Comparison of catalytic parameters of NiCoFe-TDC-AC@$NiMo_4$/MnO_{3-X} catalyst and control catalysts.

Catalysts	Substrate	Electrolyte	Cell voltage (V)@j (mA cm^{-2})	Overall stability	Reference
(Ni, Fe) S_2@MoS_2	CFP	1 M KOH	1.56@10	28 h	15
CoP/MoP@NC/CC	CC	1 M KOH	1.71@50	--	16
FeCoNi@FeNC	GC	1 M KOH	1.63@12	12 h	17
B, N:Mo_2C@BCN	NF	1 M KOH	1.84@100	20 h	18
GDY@NiFe LDH	CF	1 M KOH	1.512@20	10 h	19
CoN_x@GDY NS/NF	NF	1 M KOH	1.48@10	20 h	20
NieMoS@Co_3O_4	Cf	1 M KOH	1.57@10	50 h	21
Ni-Co-S@Ni-Co-P	NF	1 M KOH	1.57@20	20 h	22
MoS_2@Ni_3S_2	NF	1 M KOH	1.56@10	10 h	23
NiFe/$NiCo_2O_4$	NF	1 M KOH	1.67@10	10 h	24
NiCoFe-TDC-AC@$NiMo_4$/MnO_{3-X}	**NF**	**1 M KOH**	1.46@10	**80 h**	**This Work**

*Note: j: current density; NF: Ni foam; NCT: N-doped carbon nanotubes; CC: carbon cloth; CFP: carbon fiber paper; CF: copper foam; GC: Glassy carbon; Cf: carbon fiber.

Table S3 ICP result of NiCoFe-TDC-AC and electrolyte before and after stability test.

Sample	Dissolved metal (ICP)/μg		
	Ni	Co	Fe
NiCoFe-TDC-AC (before stability test)	7.84	0.87	2.94
NiCoFe-TDC-AC (after stability test)	10.6	1.20	4.07
Electrolyte (before stability test)	bld[a]	bld[a]	bld[a]
Electrolyte (after stability test)	bld[a]	bld[a]	bld[a]

[a]bld – below limit of detection.

References

1. R. Li, P. Wang, B. Chen, X. Cui, Y. Ding, Y. Li, D. Zhang, Y. Zhao and X. Zhang, *ACS Energy Lett.*, 2019, **5**, 79-86.
2. Z. Bo, Z. Xueli, V. Oleksandr, C. Riccardo, B. Michal, G.-M. Max, H. Lili, X. Jixian, L. Min, Z. Lirong, G. d. A. F. Pelayo, T. D. Cao, F. Fengjia, Y. Mingjian, Y. Emre, C. Ning, R. Tom, L. Pengfei, L. Yuhang, L. Phil De, J. Alyf, L. X. Huolin, Y. Huagui, V. Aleksandra and H. S. Edward, *Science*, 2016, **352** 5.
3. C. R. Cox, J. Z. Lee, D. G. Nocera and T. Buonassisi, *Proc. Natl. Acad. Sci. U. S. A.*, 2014, **111**, 14057-14061.
4. J.-W. Schüttauf, M. A. Modestino, E. Chinello, D. Lambelet, A. Delfino, D. Dominé, A. Faes, M. Despeisse, J. Bailat, D. Psaltis, C. Moser and C. Ballif, *J. Electrochem. Soc.*, 2016, **163**, 1177-1181.
5. Y. Gao, V. M. Le Corre, A. Gaitis, M. Neophytou, M. A. Hamid, K. Takanabe and P. M. Beaujuge, *Adv. Mater.*, 2016, **28**, 3366-3373.
6. S. Esiner, R. E. M. Willems, A. Furlan, W. Li, M. M. Wienk and R. A. J. Janssen, *J. Mater. Chem. A*, 2015, **3**, 23936-23945.
7. S. H. Kang, M. J. Jeong, Y. K. Eom, I. T. Choi, S. M. Kwon, Y. Yoo, J. Kim, J. Kwon, J. H. Park and H. K. Kim, *Adv. Energy Mater.*, 2017, **7**, 1602117.
8. J. Luo, D. A. Vermaas, D. Bi, A. Hagfeldt, W. A. Smith and M. Grätzel, *Adv. Energy Mater.*, 2016, **6**, 1600100.
9. Jingshan Luo, Jeong-Hyeok Im, Matthew T. Mayer, Marcel Schreier, Mohammad Khaja Nazeeruddin, Nam-Gyu Park, S. David Tilley, Hong Jin Fan and M. Grätzel., *Science*, 2014, **345** 1593-1596.
10. J. Gao, F. Sahli, C. Liu, D. Ren, X. Guo, J. Werner, Q. Jeangros, S. M. Zakeeruddin, C. Ballif, M. Grätzel and J. Luo, *Joule*, 2019, **3**, 2930-2941.
11. S. K. Karuturi, H. Shen, A. Sharma, F. J. Beck, P. Varadhan, T. Duong, P. R. Narangari, D. Zhang, Y. Wan, J. H. He, H. H. Tan, C. Jagadish and K. Catchpole, *Adv. Energy Mater.*, 2020, **10**, 2000772.
12. B. Eftekharinia, H. Pezeshki and A. Dabirian, *ACS Appl. Mater. Interfaces*, 2020, **12**, 17424-17435.
13. H. Park, I. J. Park, M. G. Lee, K. C. Kwon, S. P. Hong, D. H. Kim, S. A. Lee, T. H. Lee, C. Kim, C. W. Moon, D. Y. Son, G. H. Jung, H. S. Yang, J. R. Lee, J. Lee, N. G. Park, S. Y. Kim, J. Y. Kim and H. W. Jang, *ACS Appl. Mater. Interfaces*, 2019, **11**, 33835-33843.
14. Y. Kuang, M. J. Kenney, Y. Meng, W. H. Hung, Y. Liu, J. E. Huang, R. Prasanna, P. Li, Y. Li, L. Wang, M. C. Lin, M. D. McGehee, X. Sun and H. Dai, *Proc. Natl. Acad. Sci. U. S. A.*, 2019, **116**, 6624-6629.
15. Y. Liu, S. Jiang, S. Li, L. Zhou, Z. Li, J. Li and M. Shao, *Appl. Catal. B-Environ.*, 2019, **247**, 107-114.
16. Y.-J. Tang, H.-J. Zhu, L.-Z. Dong, A. M. Zhang, S.-L. Li, J. Liu and Y.-Q. Lan, *Appl. Catal. B-Environ.*, 2019, **245**, 528-535.
17. Q. Zhang, R. F. Webster, S. Cheong, R. D. Tilley, X. Lu and R. Amal, *Part. Part. Syst. Charact.*, 2019, **36**, 1800252.
18. M. A. R. Anjum, M. H. Lee and J. S. Lee, *ACS Catal.*, 2018, **8**, 8296-8305.
19. H.-Y. Si, Q.-X. Deng, L.-C. Chen, L. Wang, X.-Y. Liu, W.-S. Wu, Y.-H. Zhang, J.-M. Zhou and H.-L. Zhang, *J. Alloys Compd.*, 2019, **794**, 261-267.
20. Y. Fang, Y. Xue, L. Hui, H. Yu, Y. Liu, C. Xing, F. Lu, F. He, H. Liu and Y. Li, *Nano Energy*, 2019, **59**, 591-597.
21. Y.-N. Zhu, C.-Y. Cao, W.-J. Jiang, S.-L. Yang, J.-S. Hu, W.-G. Song and L.-J. Wan, *J. Mater. Chem. A*, 2016, **4**, 18470-18477.
22. Y. Gong, Z. Xu, H. Pan, Y. Lin, Z. Yang and J. Wang, *J. Mater. Chem. A*, 2018, **6**, 12506-12514.
23. J. Zhang, T. Wang, D. Pohl, B. Rellinghaus, R. Dong, S. Liu, X. Zhuang and X. Feng, *Angew. Chem. Int. Ed. Engl.*, 2016, **55**, 6702-6707.
24. C. Xiao, Y. Li, X. Lu and C. Zhao, *Adv. Funct. Mater.*, 2016, **26**, 3515-3523.